

SPECIAL TOPIC

Morphology-tuned phase transition of MnO₂ nanorods under high pressure

To cite this article: Xue-Ting Zhang et al 2025 Chinese Phys. B 34 066105

View the <u>article online</u> for updates and enhancements.

You may also like

- Bulk modulus of molecular crystals Xudong Jiang, , Yajie Wang et al.
- Compressive Behavior of TATB Grains inside TATB-Based PBX Revealed by In-Situ Neutron Diffraction Yi Tian, , Hong Wang et al.
- Scanning transmission electron microscopy: A review of high angle annular dark field and annular bright field imaging and applications in lithium-ion betteries.

Yu-Xin Tong, , Qing-Hua Zhang et al.

SPECIAL TOPIC — Structures and properties of materials under high pressure

Morphology-tuned phase transition of MnO₂ nanorods under high pressure

Xue-Ting Zhang(张雪婷)¹, Chen-Yi Li(李晨一)², Hui Tian(田辉)³, Xin-Yue Wang(王心悦)¹, Zong-Lun Li(李宗伦)^{2,4,†}, and Quan-Jun Li(李全军)²

¹ School of Medical Information Engineering, Shenyang Medical College, Shenyang 110034, China
 ² State Key Laboratory of High Pressure and Superhard Materials, Jilin University, Changchun 130012, China
 ³ School of Science, Shenyang Ligong University, Shenyang 110159, China
 ⁴ Spallation Neutron Source Science Center, Dongguan 523803, China

(Received 6 February 2025; revised manuscript received 15 March 2025; accepted manuscript online 18 March 2025)

The structural phase transition of MnO_2 nanorods was investigated using *in situ* high pressure synchrotron x-ray diffraction (XRD) and transmission electron microscopy (TEM). At pressures exceeding 10.9 GPa, a second-order structural phase transition from tetragonal to orthogonal, which was accompanied by fine-scale crystal twinning phenomena, was observed in MnO_2 nanorods. On account of the significant contribution of surface energy, the phase transition pressure exhibited appreciable hysteresis compared with the bulk counterparts, suggesting the enhanced structural stability of nanorod morphology. These findings reveal that the size and morphology exhibit a manifest correlation with the high pressure behavior of MnO_2 nanomaterials, providing useful insights into the intricate interplay between structure and properties.

CSTR: 32038.14.CPB.adc192

Keywords: MnO₂ nanorods, morphology, high pressure, phase transition

PACS: 61.50.Ks, 91.60.Gf, 81.10.-h, 64.60.-i

DOI: 10.1088/1674-1056/adc192

1. Introduction

structure and properties of nanomaterials show distinct differences when compared to their bulk counterparts. [1-3] Factors such as the shape, size, atomic configuration, and surface properties of nanomaterials are key to influencing the unique properties. Recently, high pressure has been explored as a method to alter the atomic arrangement and interactions, which offers a viable approach to modulating the properties of functional materials and revealing their engaging behaviors. [4-6] For instance, in materials such as TiO₂,^[7] Ho₂O₃,^[8] and Y₂O₃,^[9] particle size impacts both the structural stability during compression and the tendency to amorphize. Similarly, in compounds like Zn₂SnO₄^[10] and ZnS, [11,12] the order of phase transitions under pressure differs remarkably because of their morphology. Nevertheless, the influence of size and morphology on high pressure behavior varies among different nanosystems. Thus, a deeper exploration of how high pressure affects the properties of diverse nanomaterials in relation to their size and shape is essential for comprehensively grasping their physical and chemical characteristics.

Manganese oxides prove to be essential across a wide array of applications, covering magnetic storage, chemical catalysis, electrodes, as well as sensors. [13-16] Among these manganese oxides, MnO₂ has captured considerable interest owing

to its excellent electrical and magnetic properties. At ambient pressure, β -MnO₂ typically adopts a tetragonal phase with the space group P42/mnm, which comprises [MnO₆] octahedra with Mn²⁺ located at the center of the octahedra. [17] Research has shown the high pressure behavior of bulk β -MnO₂ within the range of 0-50 GPa, revealing a rutile to CaCl₂-type phase transition between 0.3 GPa and 8.6 GPa, [18-20] in agreement with ab initio calculations, which predict the transition to occur at approximately 5 GPa. [21] Nanostructured MnO₂ can possess diverse morphologies like plates, flowers, cubes, wires, rods, belts, hollow spheres, etc, [22-24] nevertheless, the influence of size and morphology on the compression behavior of MnO2 remains unclear. For this purpose, investigating the structural stability and phase transition of manganese oxide nanomaterials with different morphologies under high pressure offers valuable insights.

In this work, the structural properties of MnO₂ nanorods were investigated up to 41.8 GPa using *in situ* synchrotron XRD and TEM. A second-order phase transition from tetrahedral phase to CaCl₂-type structure was observed in MnO₂ nanorods above 10.9 GPa, which is higher than that reported for bulk MnO₂ in the previous literatures. This observation highlights the distinctive compression behavior of MnO₂ nanorods, which is influenced by their size and morphology. This finding contributes to a deeper understanding of the im-

[†]Corresponding author. E-mail: lizl20@mails.jlu.edu.cn

^{© 2025} Chinese Physical Society and IOP Publishing Ltd. All rights, including for text and data mining, AI training, and similar technologies, are reserved.

http://iopscience.iop.org/cpb http://cpb.iphy.ac.cn

pact of morphology and nanoscale dimensions on high pressure behaviors.

2. Experiment methods

To obtain the MnO2 nanorods of uniform size distribution, γ-MnOOH nanorods as precursor were first prepared by the hydrothermal method, then the γ -MnOOH nanorods were calcined at 400 °C in argon for 4 h for converting into MnO₂ nanorods. The samples were characterized by TEM (200 kV, HITACHI, H-8100) and high resolution transmission electron microscopy (HRTEM) (JEOL JEM-3010). High pressure was generated by utilizing a diamond anvil cell with 400-µm culet size, and 4:1 methanol-ethanol mixture was used as a pressure transmitting medium to guarantee a quasi-hydrostatic pressure environment. The gasket material used in the experiments was T301 steel, which was first pre-compressed to a thickness around 40 µm and then laser-drilled in the center to form a 110-µm diameter sample chamber. The ruby ball placed in the chamber was used to determine the pressure by using the standard fluorescent R1 peak. In situ synchrotron XRD experiments under high pressure were performed at 4W2 beamline of Beijing Synchrotron Radiation Facility (BSRF), with the incident light wavelength of 0.6199 Å. Then the Dioptas software was used to integrate the XRD images, and to convert them into diffraction patterns. Rietveld fitting of the XRD patterns was achieved in the GSAS software. [25]

3. Results and discussion

As illustrated in Fig. 1(a), the β -MnO₂ is made up of the [MnO₆] octahedron, where the Mn atom is situated at the center and coordinated with six O atoms occupying the corners of

the octahedron.^[26–28] As can be seen from Fig. 1(b), the prepared samples have regular morphology and uniform size. The diameter of the nanorods ranges approximately from 20 nm to 40 nm, and the length is about 7 µm. Figure 1(c) shows the corresponding HRTEM image of MnO₂ nanorods, the distance between the adjacent layers is 0.24 nm, corresponding to the (101) crystal plane of tetragonal phase MnO₂, which shows that the samples have a good crystallinity.

To detect the pressure-induced structural evolution, high pressure XRD measurements of MnO₂ nanorods were carried out up to 41.8 GPa. The synchrotron XRD patterns of MnO₂ nanorods at selected pressures are shown in Fig. 2(a). At lower pressure (< 10.9 GPa), all the peaks can be attributed to the P4₂/mnm space group. Upon compression, each diffraction peak gradually moves to higher angle due to lattice shrinking. When pressure increases to 10.9 GPa, the (101) and (211) diffraction peaks, which are enclosed by the dashed line, begin to widen. The enlarged images of these two diffraction peaks in the range of 8.1–13.6 GPa are shown in Figs. 2(b) and 2(c) with increasing pressure, each diffraction peak progressively splits into two, signifying the occurrence of a structural phase transition.

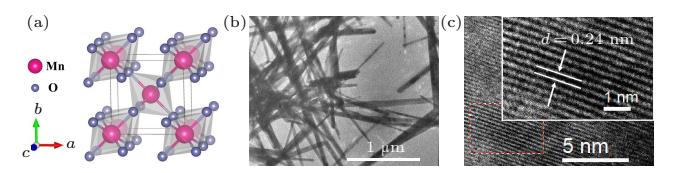


Fig. 1. Characterization of the MnO₂ nanorods with space group $P4_2/mnm$. (a) Schematic diagram of tetragonal structure, the bigger pink atoms represent Mn atoms, and the smaller blue atoms represent O atoms. (b) TEM image of the MnO₂ nanorods. (c) HRTEM image of the MnO₂ nanorods. The arrows highlight the interlayer spacing in β-phase MnO₂.

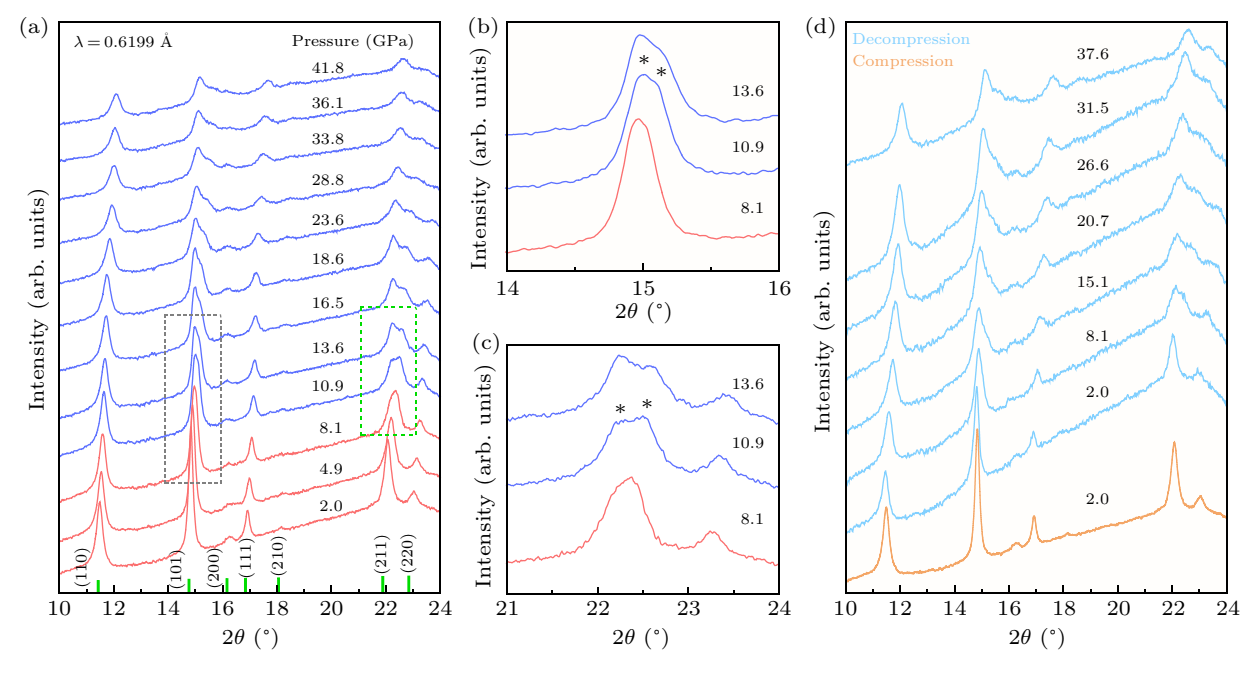


Fig. 2. (a) Synchrotron XRD patterns of MnO_2 nanorods from 2.0 GPa to 41.8 GPa upon compression. The magnified XRD patterns of the (b) (101) and (c) (211) diffraction peaks between 8.1 GPa and 13.6 GPa. (d) XRD pattern of decompression to the pressure of 2.0 GPa.

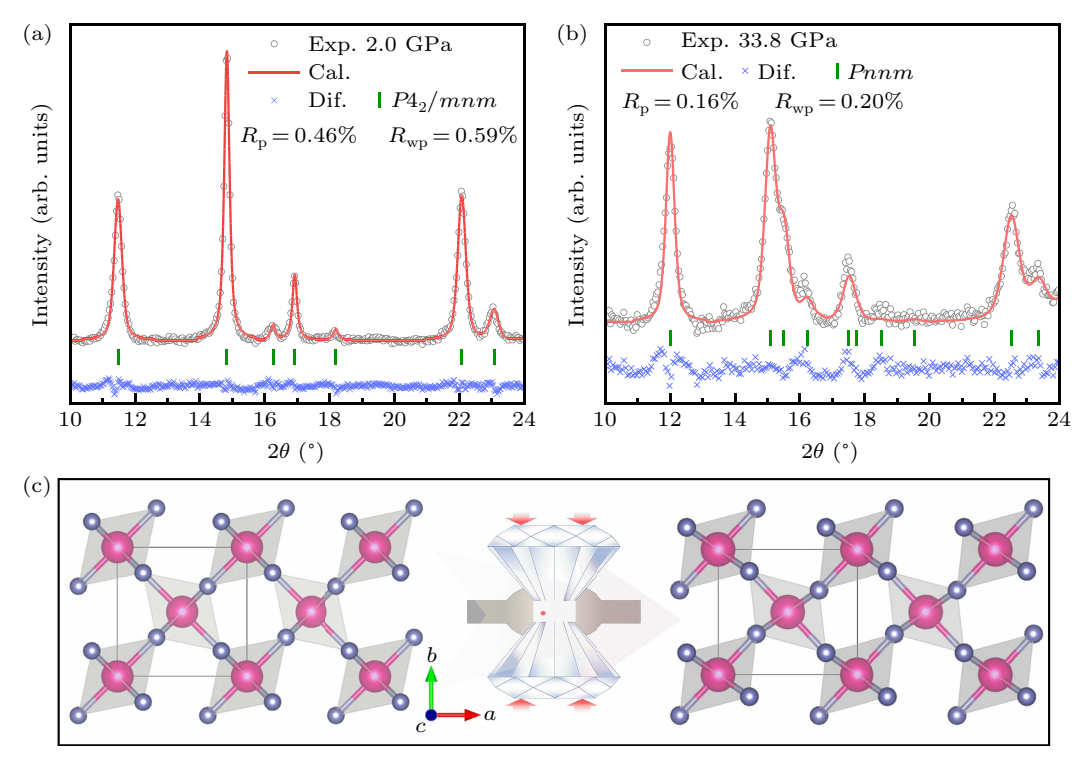


Fig. 3. Rietveld analysis of XRD pattern corresponds to (a) 2.0 GPa and (b) 33.8 GPa. (c) The schematic diagram of tetragonal phase with space group $P4_2/mnm$ and orthogonal structure with space group Pnnm, the bigger pink atoms represent Mn atoms, and the smaller blue atoms represent O atoms.

Noticeably, the transition pressure points of MnO₂ nanorods exhibit an appreciable hysteresis compared with the bulk counterparts reported by previous studies, [18-20] indicating that MnO₂ nanorods exhibit higher structural stability. The underlying reason is largely dictated by the unsaturated coordination of surface atoms and thus enhanced surface energy in MnO₂ nanorods. [29-31] In addition, the width of the diffraction peak (200) is larger than that of its adjacent peaks around 10.9 GPa, which is the result of the occurrence of fine-scale crystal twinning in this phase transition.^[18] The formation of this fine-scale crystal twinning is mainly due to the fact that the lattice parameters a and b in the tetragonal phase can become the lattice parameters b in the orthogonal phase with equal probability during the phase transition. Figure 2(d) also depicts the sample reverted to the initial rutile-type phase during decompression, indicate the phase transition of MnO2 is

As illustrated in Figs. 3(a) and 3(b), the XRD diffraction spectra of low pressure (2.0 GPa) and high pressure (33.8 GPa) were fitted by GSAS software, with their corresponding atomic structure diagrams presented in Fig. 3(c). The high pressure structure of the compressed MnO₂ nanorods is predicted based on a global minimization of free-energy surfaces using particle swarm optimization methodology as implemented in the CALYPSO code. Consistent with the previous literatures, upon compression, the octahedron of the crystal is distorted from the tetragonal phase to the CaCl₂-type structure with *Pnnm* space group. [18–20] Therefore, we believe

that the split of (101) and (211) diffraction peaks in Fig. 2 can be attributed to a structural phase transition from tetragonal to orthogonal.

Through the XRD diffraction patterns, refined lattice constants versus pressure are depicted in Figs. 4(a) and 4(b). It can be seen that the lattice constant changes discontinuously, which is consistent with the structural phase variation revealed in the XRD pattern. The lattice parameter a increases when the pressure reaches 10.9 GPa and then it remains relatively stable, which is consistent with the diffraction peak of (200) moveing to the lower angle during phase transition as shown in Fig. 2(a). While b decreases much faster than the other two lattice parameters, with a reduction of nearly 9.5%. As shown in Fig. 4(c), the volume of unit cell changes continuously upon compression, which could prove that the phase transition belongs to the second-order phase transition. [32,33] Furthermore, according to the change of cell volume with pressure, the solid line is the Birch–Murnaghan equation of state (EOS) fit to the experimental data, and a bulk modulus of 227.1(4) GPa is obtained with $V = 55.6(2) \text{ Å}^3$. Similar to the phase transition pressure, the bulk elastic modulus also differs from that of bulk MnO₂, which is 328(18) GPa.^[18,19] Previous studies indicate for a large number of materials that decrease of particle size results in an enhancement of elastic modulus. However, the difference of bulk elastic modulus between bulk materials and nano structures is considered related to the higher defect density under isotropic pressure. [34] In addition, as shown in Fig. 4(d), consistent with the previous literatures, [35,36] the abrupt change in bond length near the phase transition pressure signifies a structural reorganization, while the marked discontinuity in the Mn–O bond length further corroborates the occurrence of the phase transition of MnO₂ nanorods.

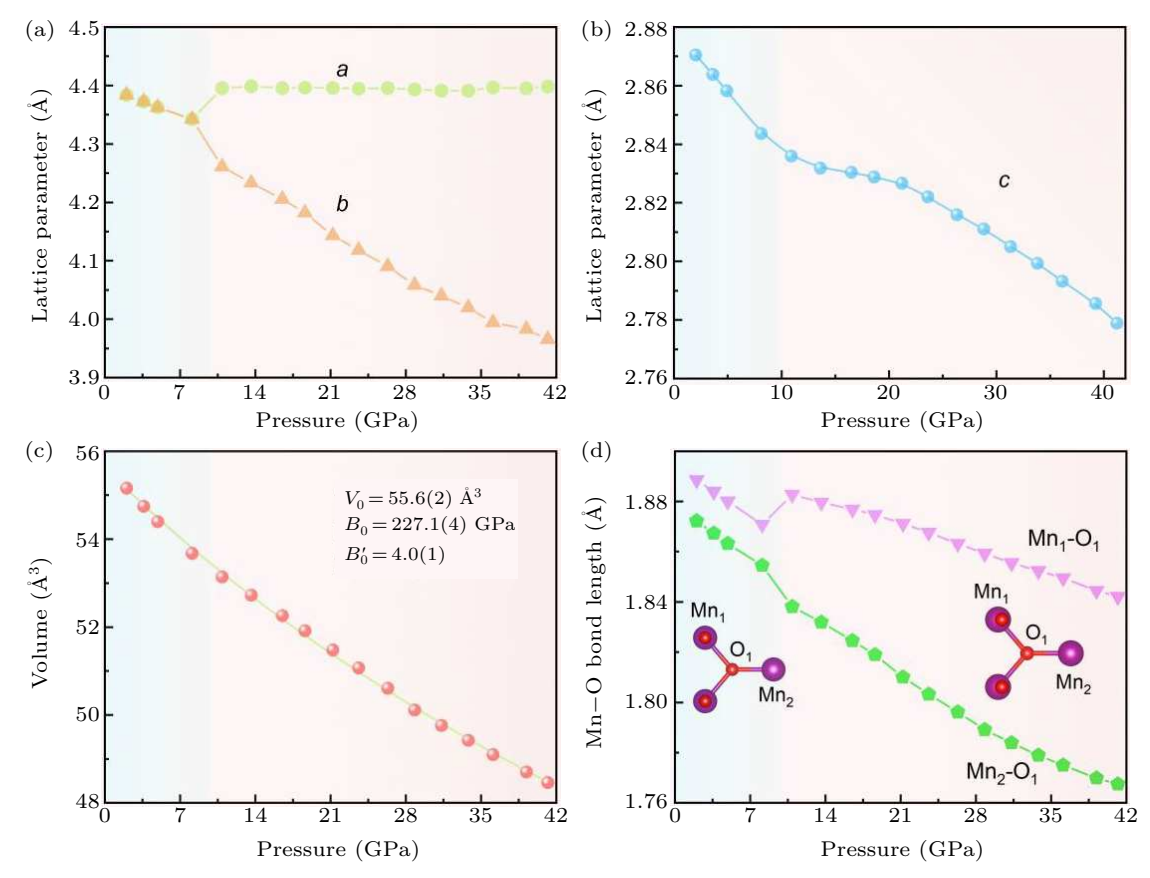


Fig. 4. The variation of MnO₂ lattice parameters (a) a, b, (b) c and (c) unit-cell volume of MnO₂ nanorods as a function of pressure. (d) Pressure-dependent variation of the Mn–O bond length.

4. Conclusion

In summary, we performed *in situ* high pressure XRD to investigate the structural evolution of MnO₂ nanorods. At around 10.9 GPa, MnO₂ nanorods transition from P4₂/mnm to Pnnm space group. The phase transition pressure of MnO₂ nanorods is higher than its bulk counterpart in consideration of the much higher surface energy in nanostructured nature, which suggests the nanorods exhibit more excellent stability. These results further suggest that the morphology and size of nanomaterials noticeably influence their behavior under high pressure, offering meaningful perspectives on the structure-property relationship.

Acknowledgments

We would like to thank Beijing Synchrotron Radiation Facility technical support groups. Project supported by China Postdoctoral Science Foundation (Grant No. 2023M742049), Guangdong Basic and Applied Basic Research Foundation (Grant No. 2023A1515110844), and the Innovative Training Program for College Students (Grant No. 20249076).

References

- Aric'o A S, Bruce P, Scrosati B, Tarascon J M and Van S W 2005 Nat. Mater. 4 366
- [2] Tan C, Cao X, Wu X, He Q, Yang J, Zhang X, Chen J, Zhao W, Han S, Nam G, Sindoro M and Zhang H 2017 Chem. Rev. 117 6225
- [3] Roduner E 2006 Chem. Soc. Rev. 35 583
- [4] Li T, Wang S, Chen X, Chen C, Fang Y and Yang Z 2024 Chin. Phys. B 33 66401
- [5] Chen J, Lv X, Li S, Dan Y, Huang Y and Cui T 2024 Chin. Phys. B 33 67104
- [6] Wang S, Zhao X, Hu K, Feng B, Hou X, Zhang Y, Liu S, Shang Y, Liu Z, Yao M and Liu B 2024 Chin. Phys. B 33 98104
- [7] Li Q, Cheng B, Tian B, Liu R, Liu B, Wang F, Chen Z, Zou B, Cui T and Liu B 2014 RSC Adv. 4 12873
- [8] Yan X, Ren X, Zhu S, Van G D, Wang L, Zhao Y and Wang S 2021 Phys. Rev. B 103 L140103
- [9] Wang L, Yang W, Ding Y, Ren Y, Xiao S, Liu B, Sinogeikin S V, Meng Y, Gosztola D J, Shen G, Hemley R J, Mao W and Mao H 2010 Phys. Rev. Lett. 105 095701
- [10] Das P P, Devi P S, Blom D A, Vogt T and Lee Y 2019 ACS Omega 4 10539
- [11] Li Z, Liu B, Yu S, Wang J, Li Q, Zou B, Cui T, Liu Z, Chen Z and Liu J 2011 J. Phys. Chem. C 115 357
- [12] Yang C, Liu Y, Sun H, Guo D, Li X, Li W, Liu B and Zhang X 2008 Nanotechnology 19 095704
- [13] Yadav P, Bhaduri A and Thakur A 2023 ChemBioEng. Rev. 10 510
- [14] Devaraj S and Munichandraiah N 2008 J. Phys. Chem. C 112 4406
- [15] Gao X, Tian D, Shi Z, Zhang N, Sun R, Liu J, Tsai H S, Xiang X and Feng W 2024 Small 20 2405627
- [16] Dou X, Chen Z, Zhang C, Li X, Qiao F, Song B, Wang S, Teng H and Lv Z 2024 Chin. Phys. B 33 114202

- [17] Clendenen R and Drickamer H 1966 J. Chem. Phys. 44 4223
- [18] Haines J, Léger J and Hoyau S 1995 J. Phys. Chem. Solids 56 965
- [19] Curetti N, Merli M, Capella S, Benna P and Pavese A 2019 Phys. Chem. Miner. 46 987
- [20] Yue B, Krug M, Sanchez V C, Merkel S and Hong F 2022 Phys. Rev. Mater. 6 053603
- [21] Li Y, Wu X, Qin S and Wu Z 2006 Chin. J. High Press. Phys. 20 285
- [22] Kaya L, Karatum O, Balamur R, Kaleli H N, Önal A, Vanalakar S A, Hasanreisoğlu M and Nizamoglu S 2023 Adv. Sci. 10 2301854
- [23] Song H, Xu L, Chen M, Cui Y, Wu C, Qiu J, Xu L, Cheng G and Hu X 2021 RSC Adv. 11 35494
- [24] Gaikwad N K, Kulkarni A A, Beknalkar S A, Teli A M and Bhat T S 2024 J. Energy Storage 100 113418
- [25] Toby B 2001 J. Appl. Crystallogr. 34 210
- [26] Zhu S, Li L, Liu J, Wang H, Wang T, Zhang Y, Zhang L, Ruoff R S and Dong F 2018 ACS Nano 12 1033
- [27] Zhan D, Zhang Q, Hu X and Peng T 2013 RSC Adv. 3 5141
- [28] Wang G, Nie L and Yu S 2012 RSC Adv. 2 6216

- [29] Baranov A N, Sokolov P S, Tafeenko V A, Lathe C, Zubavichus Y V, Veligzhanin A A, Chukichev M V and Solozhenko V L 2013 Chem. Mater. 25 1775
- [30] Chen Z, Li G, Zheng H, Shu X, Zou J and Peng P 2017 Appl. Surf. Sci. 420 205
- [31] Xiao G, Yang X, Zhang X, Wang K, Huang X, Ding Z, Ma Y, Zou G and Zou B 2015 J. Am. Chem. Soc. 137 10297
- [32] Du X, An C, Chen X, Zhou Y, Zhang M, Wang S, Chen C, Zhou Y, Yang X and Yang Z 2023 *Phys. Rev. B* 108 014109
- [33] Tian C, Huang X, Gao Y, Tian F, Liang M, Fang Y, Huang F and Cui T 2023 Phys. Rev. B 108 L180507
- [34] Yue L, Xu D, Wei Z, Zhao T, Lin T, Tenne R, Zak A, Li Q and Liu B 2022 Materials 15 2838
- [35] Paris E, Joseph B, Iadecola A, Marini C, Ishii H, Kudo K, Pascarelli S, Nohara M, Mizokawa T and Saini N L 2016 Phys. Rev. B 93 134109
- [36] Cuartero V, Monteseguro V, Otero de la Roza A, El Idrissi M, Mathon O, Shinmei T, Irifune T and Sanson A 2020 Phys. Chem. Chem. Phys. 22 24299